- Technical Paper -

EFFECT OF REINFORCEMENT ARRANGEMENT ON STRUCTURAL PERFORMANCE OF DAPPED-END BEAMS

Wanakorn PRAYOONWET[*1], Yasuhiko SATO[*2], and Wanchai Yodsudjai[*3]

ABSTRACT

The structural performance of dapped-end beams, reinforced with either diagonal or hanger rebars in the disturbed region, is investigated through nonlinear finite element analysis. The results indicate that a dapped-end beam reinforced with diagonal rebars shows greater capacity, stiffness, and crack restraint compared to one reinforced with hanger rebars. However, excessive horizontal cracking at the re-entrant corner may occur when using only diagonal rebars under higher load levels. Therefore, an enhanced structural design of the dapped-end beam is suggested by integrating both diagonal and hanger rebars.

Keywords: dapped-end beams, reinforcement arrangement, structural performance, structural design

1. INTRODUCTION

Dapped-end beams (DEBs) have widely been utilized in the construction of concrete structures. The upper nibs of main girders are supported by the beam-ledges or corbels of the adjacent girders or substructures. As a result of the reduction in the overall height of girders' sections near the supports, there is a subsequent decrease in the total construction height. Also, the enhancement in lateral stability at supports can be achieved by using this structural configuration [1].

Typically, the layouts of reinforcement details in DEBs used worldwide can be categorized into two main categories as illustrated in Fig. 1. In the first approach, the diagonal reinforcements (DR) are utilized to transfer the reaction forces from upper nibs to the full-depth sections. This reinforcement detail is commonly used in Europe and designed by means of a strut-and-tie model (STM) suggested by BS EN 1992 [2]. A second approach, which is widely implemented in the US, emphasizes on the application of main nib flexural reinforcements together with the hanger rebars (HR) located near by the end face of full-depth sections. The design can be conducted based on STM [3] or simplified equations provided by the PCI design handbook [4].

Although many previous studies indicated that the DEBs designed following either two approaches satisfied the codified requirements of both service limit state (SLS) and ultimate limit state (ULS) [1,5], the number of papers discussing on advantages and shortcomings of different dapped-end reinforcement arrangements at each limit state are limited.

Therefore, to further enrich the knowledge of structural design, the analytical study using the three-dimensional nonlinear finite element method (3D-NLFEM) has been conducted to clarify the impact of rebar arrangements on the structural performance at SLS, ULS, and maximum loading state. The study aims to compare the overall behaviors, crack development, and rebars strain resulted from different reinforcement details in the disturbed region (D-region). The findings from this study will serve as a basis for enhancing the design and arrangement of reinforcements in the DEBs.

2. DESIGN OF ANALYTICAL INVESTIGATION

2.1 Structural configurations

The target structure is a simply supported pretensioned I-girder typically employed in Thailand for the construction of bridge superstructures. Originally, the reinforcement detail in a D-region of a dapped-end beam (DEB) was designed according to the PCI standard [4], as depicted in Fig. 1a. Subsequently, to delve into the impacts of reinforcement arrangement, the rebar layout of the D-region in existing DEB was re-designed as per the BS EN 1992 [2]. The final detail is shown in Fig. 1b. It is worth mentioning that ribbed deformed reinforcing bars (DB) were utilized as ordinary reinforcements in both analyzed DEBs. For the concrete cover between normal rebars and concrete surface, a clear cover of 25 mm is maintained in all DEBs.

2.2 Materials

The same material properties are possessed by two DEBs having different rebar arrangements. Table 1 summarizes the properties of ordinary and prestressing reinforcements, while the concrete properties are tabulated in Table 2. Also, at supports and loading position, steel plates having elastic modulus of 200000 N/mm^2 were applied in all analyses to prevent stresses concentration. It is important to note that these material properties were implemented throughout this study.

*1 Graduate School of Creative Science and Engineering, Waseda University, JCI Student Member
*2 Professor, Dept. of Civil and Environmental Engineering, Waseda University, Ph.D., JCI Member
*3 Professor, Dept. of Civil Engineering, Kasetsart University, Ph.D.

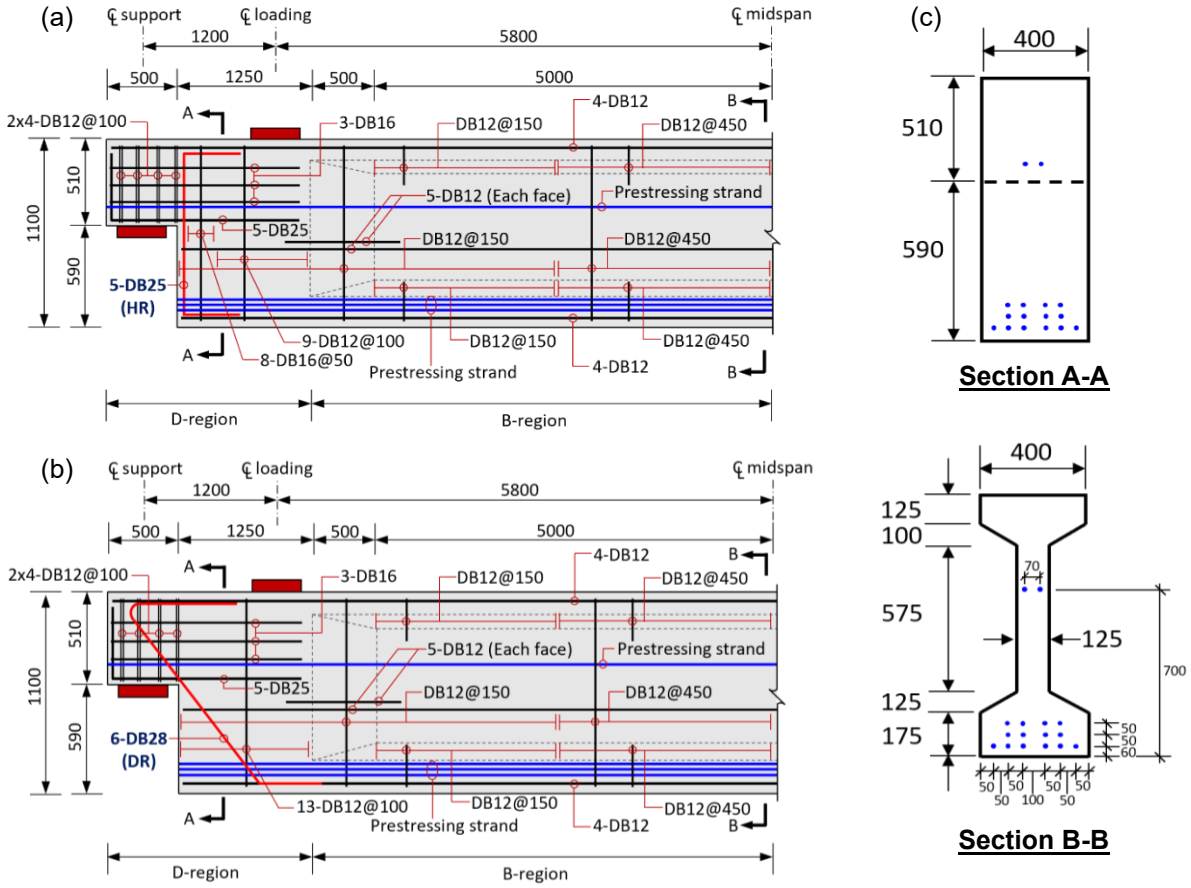

Fig.1 Reinforcement layouts and dimensions of DEBs; (a) Arrangements according to the original design, (b) Arrangements following the BS EN 1992, and (c) Cross-section detail (dimensions are in millimeters)

Table 1 Properties of reinforcements

Type	Elastic modulus (N/mm^2)	Yield strength (N/mm^2)	Tensile strength (N/mm^2)
Deformed bars	200000	295	480
7-wire strands	196000	1581	1860

Table 2 Properties of concrete

28-day cylinder compressive strength (N/mm^2)	Elastic modulus (N/mm^2)
35	34350

2.3 Finite element modeling

(1) Modeling strategy

A nonlinear finite element analysis of DEBs was performed using a commercial software 3D ATENA. The analyses aimed to examine the structural behaviors and responses at SLS, ULS, and failure state.

The applied load was divided into two stages in the analysis. In the first loading stage, the girder's self-weight and prestressing force considering the effects of instantaneous and long-term losses were loaded to the DEBs. Then, the displacement-controlled load was incrementally applied at the distance of 1200 mm measured from the centerline of pin support on the left side of DEBs. It is important to note that prior to defining this loading position, the displacement-controlled loading force was applied in incremental location between 1100 and 1500 mm measured from a pin support to ensure the occurrence of a failure within the D-region of a DEB. It was observed that the shear failure within the nib and full-depth sections occurred when the applied loads were between 1100 and 1200 mm. Once the loading forces were further from this point, the failure mode was changed from the shear cracks within the D-region to the flexure-shear cracks with concrete crushing at the loading point. The observed minimal reaction force to induce the shear failure within the D-region occurred when the loading location was optimized to 1200 mm from the centerline of a pin support. Therefore, this loading position was employed in the current study as it provided the minimal shear capacity while preserving shear failure at the nib and full-depth sections.

In the numerical simulation, a modified Newton-Raphson was implemented for the nonlinear analysis. Throughout the meshing process, the element size of 50 mm was used in all regions of the target structures. This resulted in 11-layer and 23-layer through the depth of nibs and full-depth section of DEBs, respectively.

The structural concrete was modeled using brick elements and tetrahedral elements with linear interpolation function. The former was applied to all regions of DEBs retaining rectangular geometry,

whereas the latter was used in all other areas when the brick elements were inappropriate. For the ordinary reinforcements in the nibs of DEBs and prestressing steels, the modeling process was achieved using the discrete two-dimensional (2D) truss bar elements, whereas the reinforcements located in other zones were modeled with a smeared reinforcement approach. Also, at the support and loading position, the steel plate was modeled using the tetrahedral elements. Further details regarding specific properties of elements are referred to the ATENA user manual [6]. The example of numerical model together with reinforcements is presented in Fig. 2.

(2) Material constitutive laws

To simulate the behavior of concrete subjected to different stress states, the constitutive law developed based on the fracture-plastic model is needed. Therefore, the equivalent uniaxial stress-strain law considering concrete behavior in tension and compression at pre-peak and post-peak was utilized according to the ATENA user manual [6]. For tension softening of concrete, the exponential crack opening law suggested by Hordijk incorporating with the crack band theory was employed. For the triaxial stresses state in concrete, the fracture model formulation was constructed using the Rankine failure criterion together with the plasticity model based on the Menétrey-William failure surface [6].

To model the behavior of the ordinary and prestressing reinforcements under different stress states, the bi-linear, elastic-perfectly plastic, stress-strain law was implemented. In this study, to solely emphasize the impacts of reinforcement arrangements on structural performance, the assumption of perfect bond between concrete and reinforcements was employed in all analyses. Also, the linear behavior of steel plates was modeled using 3D-elastic isotropic constitutive law.

3. COMPARISON BETWEEN TWO DEBs

3.1 Overall behaviors

DEBs possessing different rebar arrangements were loaded until failure. At each load increment, the reaction force at nib and deflection at the re-entrant corner located close to the applied load were monitored. Then, their relationship was drawn as shown in Fig. 3. Obviously, the load-bearing capacity and stiffness of the DEB reinforced with DR were larger than that reinforced with HR. The maximum load-carrying capacity of 1599 kN was obtained from the design as per the BS EN 1992, while the recorded peak-load of another one using HR was 1072 kN. Furthermore, the observed deflection at maximum load-bearing capacity from two dapped-end girders was significantly different. The deflection at re-entrant corner depicted from a design using the DR was 4.27 mm, which is 1.43 times higher than the DEB reinforced with the HR.

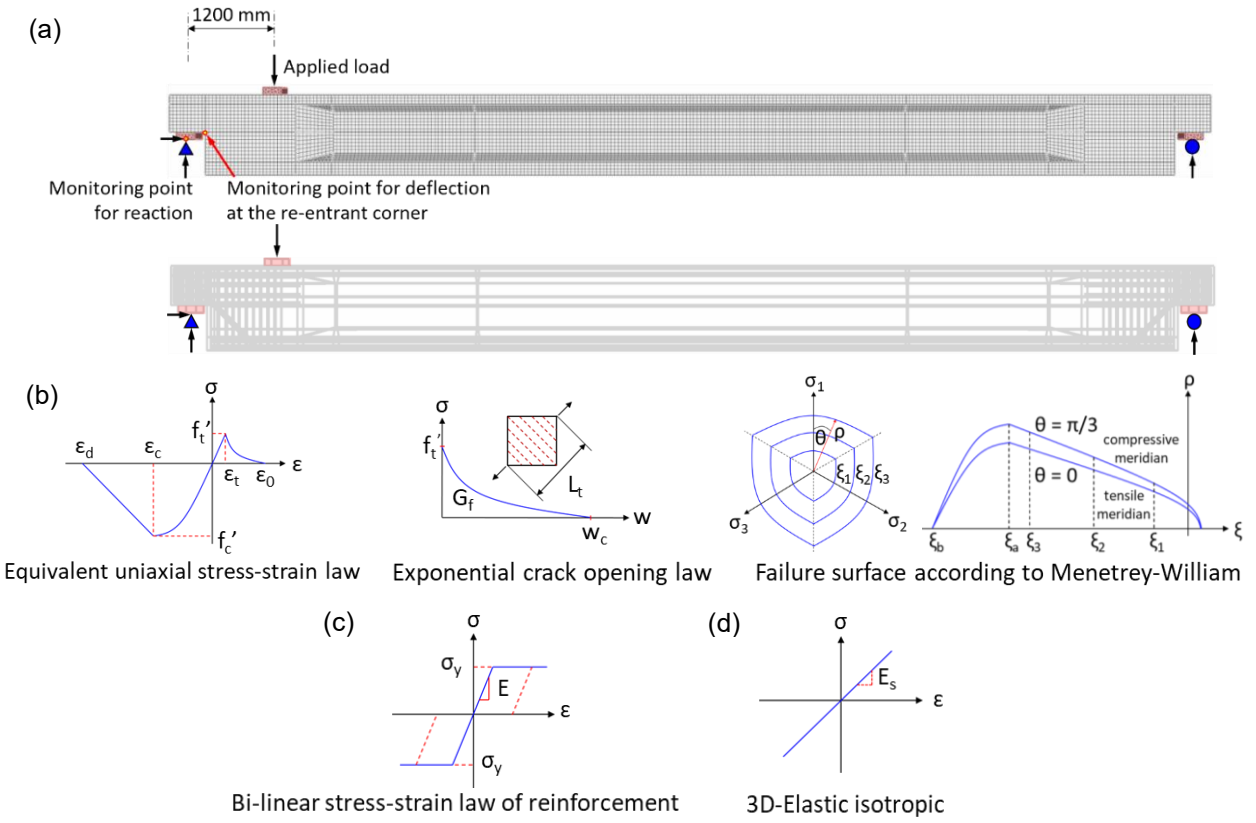

Fig.2 Representation of nonlinear finite element model; (a) Finite element mesh detail and discrete reinforcement modelling, (b) Constitutive laws for concrete, (c) Reinforcement stress-strain law, and (d) 3D-elastic isotropic for stress-strain in steel plate

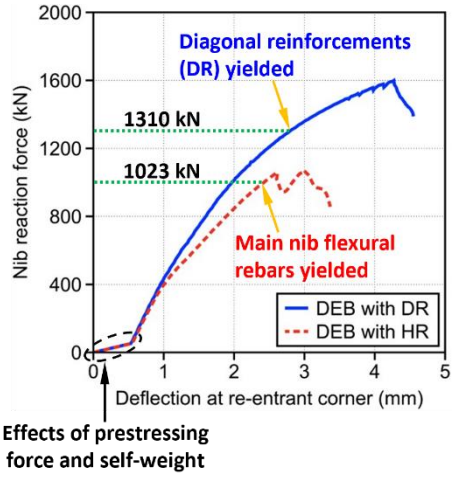

Fig.3 Relationship between reaction force at nib and deflection at re-entrant corner

Based on Fig. 3, it suggested that the load-carrying capacity and ductility performance of the DEB reinforced with DR were superior to the design utilizing HR. This result conformed to previous studies [1,5]. It is worth noting that in Fig. 3, the deviation at the beginning of the curve was induced by the effects of prestressing force and self-weight in the DEB, provided in the first loading stage of the analyses. In general, DR was placed 45 degrees to the longitudinal axis of DEBs. Owing to this arrangement, the DR can effectively resist the diagonal tensile stresses in the nib. Thus, better structural resistance and deflection accommodation at nib section can be accomplished compared to the use of HR.

3.2 Crack development

The comparison of crack development between DEBs reinforced with DR and HR in each limit state [7] was demonstrated in Fig. 5. Once, the reaction force reached the SLS load level of 590 kN, the cracks at the re-entrant corner of both DEBs were widened and propagated towards top faces and full-depth sections of DEBs (Fig. 5a). It can be detected that in the DEB reinforced with the DR, the maximum crack width ($w_{cr,max}$) was narrower compared to another design using the HR, and the cracks were less propagated. Nonetheless, both observed crack widths were smaller than maximum allowable crack widths limited by the BS EN 1992 [2] and the AASHTO LRFD bridge design specification [7]. In this research, the crack width (w) can be calculated based on the principle of crack band theory and principal tensile strain [6]. The equation can be expressed as follows:

$$w = \varepsilon_{cr} L_t' \quad (1)$$

$$L_t' = \gamma L_t \quad (2)$$

$$\gamma = 1 + (\gamma^{max} - 1)\theta/45 \quad (3)$$

where,

w : crack width (mm)

ε_{cr} : principal tensile strain

L_t : failure band in tension (mm)

L_t' : failure band with element orientation effect

γ : linear interpolation function ($\gamma^{max} = 1.5$)

θ : minimal angle between the direction perpendicular to failure plane and element side ranged from 0 to 45 degrees

It is noteworthy that the possible failure plane can be estimated based on the tensor of principal strain obtained from the finite element analysis as illustrated in Fig. 4.

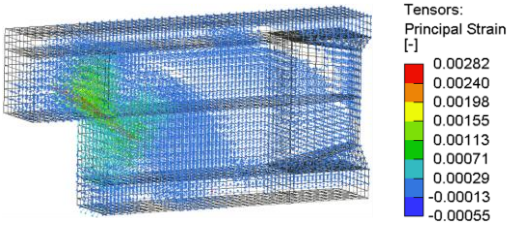

Fig.4 Example of principal strain tensor at SLS

When the load increment induced the reaction force at nibs corresponding to the ULS load level (911 kN), the enlargement of crack width and crack propagation at nib and full-depth sections can be visible from both DEBs as illustrated in Fig. 5b. At the maximum loading state (Fig. 5c), in general, both target DEBs exhibited nib shear failure together with shear failure at the full-depth section. Nevertheless, for the DEB designed with DR, the failure was induced by shear failure incorporating with large horizontal crack at the re-entrant corner.

Based on the results of crack development, they further highlighted that the implementation of DR provides advantage in diagonal tension force resistance for the DEB since the rebars' direction was compatible with diagonal tensile stresses. Additionally, these reinforcements were placed perpendicular to diagonal crack planes leading to much better crack restraint compared to the use of HR. However, in the DEB reinforced with the DR, the horizontal crack was substantially widened compared to the design using HR due to the absence of vertical ties near the re-entrant corner.

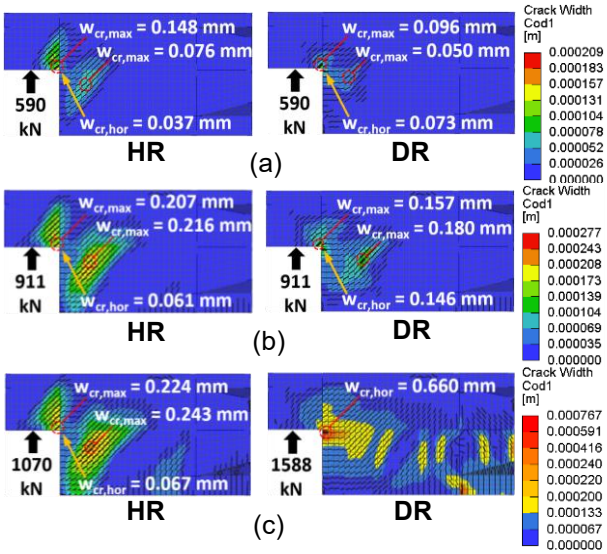

Fig.5 Crack development in each limit state; (a) SLS, (b) ULS, and (c) Maximum loading state

3.3 Strain in reinforcements

The tensile strain in main reinforcements of both target DEBs was examined. In the DEB designed according to BS EN 1992 standards, yielding of reinforcement was observed within the DR, as depicted in Fig. 6a. The yielding strain of the rebar, which is equal to 0.00148, was reached when the nib reaction force reached 1310 kN, as indicated in Fig. 3. On the contrary, the response of main nib flexural reinforcements remained within an elastic range throughout the analysis. This observation suggests that the DR not only resists diagonal tensile stresses, but also flexural stresses induced by the bending moment at the nib. Consequently, the yielding of main nib flexural reinforcement is prevented in the DEB featuring DR. Therefore, the maximum load-carrying capacity of this DEB can be increased as the reserved capacity is provided by the main nib flexural reinforcements. On the other hand, for the DEB designed as per the PCI design handbook, yielding of main nib flexural reinforcements was detected and initiated at the reaction force of 1023 kN, as noted in Fig. 3, while the yielding state of HR could not be detected throughout the analysis, as shown in Fig. 6b.

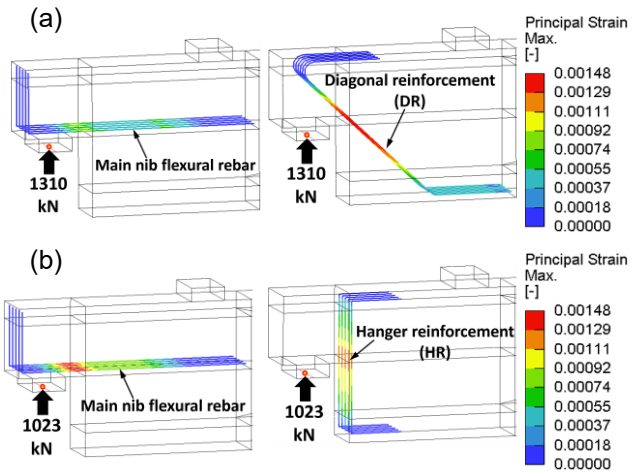

Fig. 6 Strain in reinforcement; (a) main nib flexural rebars and diagonal rebars in DEB featuring DR, and (b) main nib flexural rebars and hanger rebars in DEB featuring HR

4. REBAR ARRANGEMENT ENHANCEMENT

Based on previous analytical results, the authors have suggested to integrate both DR and HR in the DEB, which is a common practice in Japan, so as to improve the reinforcing effect in the nib. This arrangement aimed to leverage nib's tensile stresses resistance and diagonal crack restraint through the DR. Additionally, the horizontal crack at the re-entrant corner can be mitigated using the HR as a vertical tension tie.

The number of reinforcements necessary to ensure structural strength was designed considering two parallel structural systems comprising HR and DR. Subsequently, one-half of the reaction force at ULS was assigned to each system to calculate the required number of DR and HR according to the BS EN 1992 [2] and the PCI design handbook [4], respectively. For other reinforcements within the D-region, one-half of the required number of reinforcements, determined from each structural system, was added together. The finalized rebar layout is shown in Fig. 7. It is important to note that the reinforcement arrangement must be consistent with the stress field in each structural system to ensure correct load-transferring mechanism and sufficient load-carrying capacity at ULS, as well as to limit crack development under service load conditions.

The comparison of crack development, resulting from DEBs with different rebar layouts under various limit states, is illustrated in Fig. 8. For SLS, the $w_{cr,max}$ at re-entrant corner was 0.119 mm for a DEB reinforced with both DR and HR. This value lied between the smallest (0.096 mm) and largest (0.148 mm) crack widths obtained from the designs using only DR or HR, respectively.

The combined utilization of DR and HR demonstrated a significant impact at ULS load level. The diagonal crack was kept from opening through DR. The $w_{cr,max}$ was 0.158 mm in the full-depth section. For the horizontal crack at re-entrant corner, HR drastically narrowed down this crack from 0.146 mm (DR only) to 0.074 mm (combined DR and HR). Subsequently, at the peak-loading state, the primary cause of failure was the nib shear failure and the widened shear crack in the full-depth section, with negligible influence from the horizontal crack at the re-entrant corner.

Compared to the DEB featuring only HR, the utilization of both DR and HR can significantly enhance load-bearing capacity and stiffness of the DEB, as illustrated in Fig. 9. In terms of stiffness, a DEB reinforced with combined DR and HR exhibited comparable performance to that reinforced solely with DR.

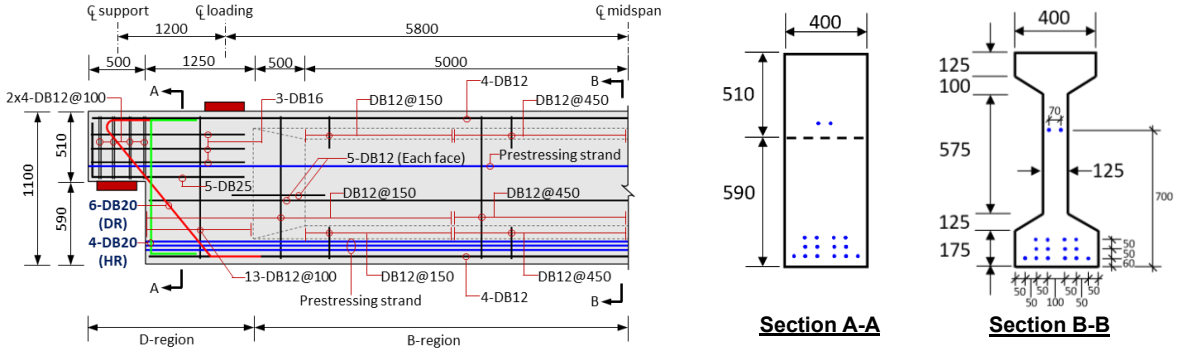

Fig. 7 Rebar layout of combined DR and HR in DEB and cross-section (dimensions are in millimeters)

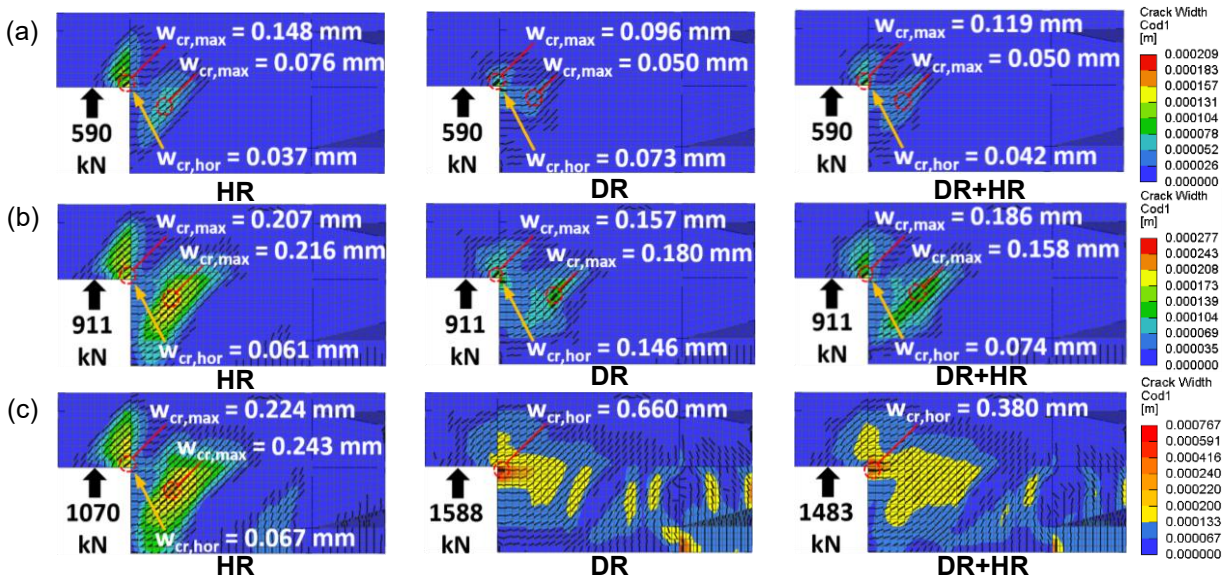

Fig. 8 Comparison of crack development; (a) SLS, (b) ULS, and (c) Maximum loading state

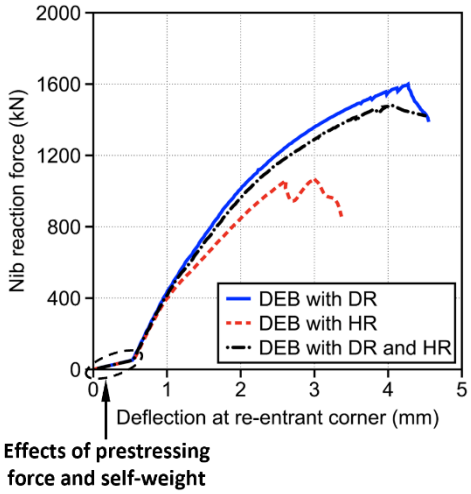

Fig. 9 Comparison of reaction force and deflection at re-entrant corner relationship among three nibs

5. CONCLUSIONS

The effects of reinforcement arrangements on the structural performance of DEBs were investigated through the numerical analyses of DEBs reinforced with either DR or HR. Subsequently, the proposal for integrating DR and HR to enhance the structural design methodology was presented. Based on the findings, following conclusions can be drawn:

(1) A DEB reinforced with DR exhibited greater load-carrying capacity and stiffness than that reinforced with HR since the 45-degree arrangement of DR was compatible with the diagonal tensile stresses.

(2) DR showed superior performance to HR in terms of diagonal crack restraint since their placement was perpendicular to diagonal crack planes. However, the lack of vertical tension ties (HR) near the re-entrant corner resulted in excessive widening of horizontal cracks at the re-entrant corner under higher load levels.

(3) The integrated utilization of DR and HR can improve the structural performance of the DEB. The presence of both rebars resulted in better load-carrying capacity and stiffness compared to the conventional use of only HR. Furthermore, the observed diagonal cracks in nib and full-depth sections and horizontal cracks at the re-entrant corner were effectively restrained by the combined use of DR and HR, respectively.

ACKNOWLEDGEMENT

The authors acknowledge the fundings support provided by JICA-SATREPS for this research.

REFERENCES

[1] Mohammed, B.S., Muhammad, A., Liew, M.S., and Wan Abdullah Zawawi, N.A., "Structural performance of RC and R-ECC dapped-end beams based on the role of hanger or diagonal reinforcements combined by ECC," Int. J. Concr. Struct. Mater., Vol.13 (44), Sep. 2019.

[2] BS EN 1992-1-1. "Eurocode 2: Design of Concrete Structures,". 2004. pp.181.

[3] Mattock, A.H., "Strut-and-tie models for dapped-end beams,". Concr Int., Vol.34 (2), pp.35–40, Feb. 2012.

[4] Precast/Prestressed Concrete Institute. "PCI design handbook 7th ed.,". 2010. pp.301-305.

[5] Desnerck, P., Lees, J.M., and Morley, C.T., "Impact of the reinforcement layout on the load capacity of reinforced concrete half-joints,". Eng Struct., Vol.127, pp.227-239, Nov. 2016.

[6] Červenka, V., Jendele, L., and Červenka, J., "ATENA program documentation. Part 1: Theory,". 2011. pp.15-99.

[7] AASHTO, "AASHTO LRFD bridge design specification 9th ed.,". 2020. pp.16-341